THE JOURNAL OF PHYSICAL CHEMISTRY C

Article

Cite This: J. Phys. Chem. C 2019, 123, 27172−27180

pubs.acs.org/JPCC

Noncentrosymmetric Sulfide Oxide MZnSO (M = Ca or Sr) with Strongly Polar Structure as Novel Nonlinear Crystals

Ali H. Reshak,*[,†,‡,§] Nada M. Abbass,[∥] Jiri Bila,[§] Mohd R. Johan,[‡] and Ivan Kityk[⊥,#]

[†]Physics department, College of Science, Basrah University, Basrah 61004, Iraq

[‡]Nanotechnology and Catalysis Research Center (NANOCAT), University of Malaya, Kuala Lumpur 50603, Malaysia

[§]Department of Instrumentation and Control Engineering, Faculty of Mechanical Engineering, CTU in Prague, Technicka 4, Prague 6 166 07, Czech Republic

[∥]Department of Chemistry, College of Science, Baghdad University, Jaderiya, Baghdad 10071, Iraq

[⊥]Department of Experimental Physics and Information-measuring Technology, Lesya Ukrainka Eastern European National University, Voli Avenue 13, Lutsk 43025, Ukraine

[#]Institute of Optoelectronics and Measuring Systems, Czestochowa University of Technology, Armii Krajowej 17, Czestotchowa 42-201, Poland

Supporting Information

ABSTRACT: We performed a comprehensive ab inito calculation to investigate the influence of substitution of Ca^{2+} (180 pm) by larger Sr^{2+} (200 pm) in MZnSO (M = Ca or Sr) on the structural properties and, hence, on the linear and nonlinear optical properties. The substitution of Ca^{2+} by Sr^{2+} in MZnSO causes a band gap reduction resulting in an influence on the photophysical properties and enhances the optic activity toward the visible region. The observation of linear optical properties reveals a band gap reduction on moving from Ca to Sr, and the whole spectral structure shifts toward lower energies. The substitution of Ca^{2+} by Sr^{2+} introduces an obvious enhancement in the anisotropy between the extraordinary and ordinary tensor components, as confirmed by the uniaxial anisotropy and birefringence favoring an important role in second harmonic generation (SHG) and optical parameter oscillator due to better fulfilling of phase-matching conditions. The calculations show that SrZnSO exhibits larger SHG and microscopic first hyperpolarizability (β_{ijk}) than CaZnSO.

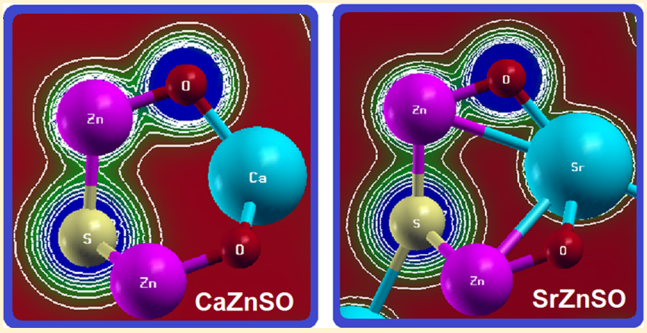

1. INTRODUCTION

Nonlinear optical (NLO) crystals are essential materials for generation of coherent light and are used in laser frequency conversion, optical parameter oscillator (OPO), and other optical and photonic devices.[1−10] The role of NLO crystals is to generate tunable laser beams covering the various optical spectra regions by means of frequency conversion. The commercially available crystals are capable of harmonic generation in the region from UV to near-IR. Efforts have been made to grow high-quality crystals to improve their laser performance in practical applications and to discover new crystals to extend the spectra coverage into deep-UV and mid-IR region. Borate crystals have attracted considerable interest due to their important application in second harmonic generation (SHG).[1−17] Usually, a noncentrosymmetric structure consisting of asymmetric or polar structural units exhibits a large SHG response.[18] For example, the large SHG effects of β-BaB_2O_4[19] and LiB_3O_5[20] are mainly contributed by the planar polyanions $(B_3O_6)^{3-}$ and $(B_3O_7)^{5-}$, respectively.

Kang et al.[21] have used the first-principles theory for designing two novel NLO carbonates $KBeCO_3F$ and $RbAlCO_3F_2$. The investigated crystals are structurally stable, and they possess very large energy band gaps and considerable optical anisotropy. They reported that $KBeCO_3F$ and $RbAlCO_3F_2$ are very promising deep-UV NLO crystals alternative to potassium beryllium fluoroborate (KBBF). The recent experimental results on $MNCO_3F$ (M = K, Rb, Cs; N = Ca, Sr, Ba)[22] suggest that the synthesis of the $KBeCO_3F$ and $RbAlCO_3F_2$ crystals is feasible. Liang et al.[23] have investigated the usage of metal sulfides with diamond-like (DL) structure for NLO applications in the mid-IR spectral region. The linear and NLO properties of the DL-metal sulfides are analyzed on the basis of first-principles calculations. It has been found that it is relatively easy to achieve good balance between the band gap and the NLO performance. Moreover, the moderate

Received: September 19, 2019
Revised: October 11, 2019
Published: October 18, 2019

DOI: 10.1021/acs.jpcc.9b08766
J. Phys. Chem. C 2019, 123, 27172−27180

birefringence Δn (~0.03−0.10) is crucial for practical mid-IR NLO applications. They reported that several metal sulfides with normal DL and defect DL structures show excellent mid-IR NLO properties. These studies provide useful information for the design and discovery of novel materials possessing good mid-IR NLO performance. Lin et al.[24] have reported that the ab initio approaches have the ability to accurately predict the optical properties of NLO crystals and that the developed analytic tools are very important to explore their intrinsic mechanism. This microscopic understanding is crucial for designing novel crystals with large NLO properties. It is expected that the first-principles approaches will deeply enhance the search efficiency and help the researchers to save resources in the exploration of novel NLO crystals with good performance.

Sambrook et al.[25] have synthesized a pure CaZnSO compound that crystallized in a noncentrosymmetric hexagonal space group ($P63mc$) with two formula per unit cell. The reported lattice constants are a = 3.75726(3) Å and c = 11.4013(1) Å. They have measured the powder SHG level using a 1064 nm laser radiation. The efficiency of CaZnSO is approximately 100 times that of α-SiO_2, and the piezoelectric coefficient is as high as 38 pm V^{-1}. They reported that the substitution of Ca^{2+} (180 pm) by larger Sr^{2+} (200 pm) in CaZnSO introduces a different chemical pressure, which can change the structural polarity and energy band gap. At the same time, they reported that is it not possible to synthesize an analogue SrZnSO. Very recently, Liu et al.[26] successfully synthesized a novel polar SrZnSO compound crystallized in a noncentrosymmetric hexagonal space group ($P63mc$) with lattice parameters a = 3.90442(6) Å, c = 11.6192(2) Å, and Z = 2. They have found that SrZnSO is isostructural to CaZnSO and is less polar than CaZnSO, but they did not measure the SHG signal of SrZnSO. We should emphasize that the previous study[25] reported the SHG value for the CaZnSO powder without taking into account the influence of the packing structural units. We would like to highlight that, on the basis of anionic group theory,[27] the overall SHG response of a crystal is the geometrical superposition of the second-order susceptibilities. Therefore, the packing of the MS_3O_3 octahedra and ZnS_3O tetrahedra structural units may also affect the macroscopic SHG coefficients.[28] The large SHG is due to the strong interactions between the MS_3O_3 octahedra and ZnS_3O tetrahedra.[28] Thus, the reported values of the SHG have been only estimated for powder samples without taking into account the influence of the packing of the MS_3O_3 octahedra and ZnS_3O tetrahedra structural units. Hence, we have addressed ourselves to calculating the SHG of the MZnSO (M = Sr or Ca) single crystals, taking into account the influence of the packing of the MS_3O_3 octahedra and ZnS_3O tetrahedra structural units using the full-potential method. We emphasize that in full-potential method, the potential and charge density are expanded into lattice harmonics inside each atomic sphere and as a Fourier series in the interstitial region. This has a profound effect on the electronic structure as well as on linear and nonlinear optical properties and needs to be studied. Therefore, we thought that it would be interesting to perform full-potential calculations using the recently modified Becke−Johnson potential (mBJ)[29] and investigate the influence of Ca^{2+} substitution by Sr^{2+} on the linear and nonlinear optical properties and microscopic first hyperpolarizability of sulfide oxide MZnSO (M = Ca or Sr).

2. STRUCTURAL ASPECT AND METHODOLOGY

The structural features of MZnSO (M = Sr or Ca) consist of close-packed sulfur and oxygen layers in *hc* stacking: M in octahedral and Zn in tetrahedral voids. The infinite layers of edge-linked MS_3O_3 octahedra and infinite layers of vertex-linked ZnS_3O tetrahedra share sulfur−sulfur edges and oxygen vertices to form a three-dimensional framework.[25,26] The crystal structure of MZnSO (M = Ca or Sr) has polar layers in the *ab* plane sharing ZnS_3O tetrahedra that are separated by M ions of the MS_3O_3 octahedra.[26] It is clear that the substitution of Ca by larger Sr causes an influence on the bond lengths (Figure 1a), and this may lead to an influence on the electronic properties. The distribution of the electron clouds around the neighboring atoms is shown in Figure 1b,c). In Figure 1c, it is shown that Sr shares the outer shells with ZnS_3O tetrahedra.

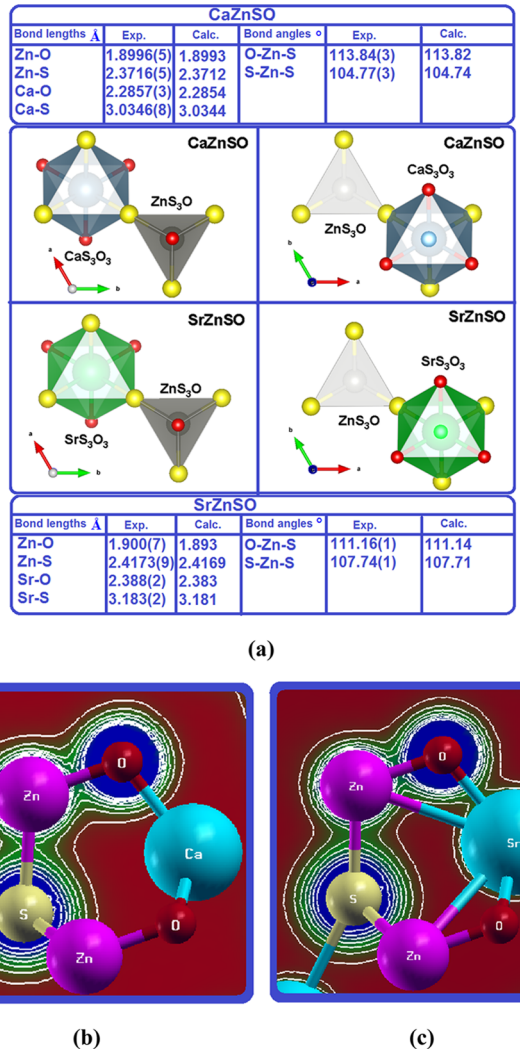

Figure 1. (a) Crystal structure of MZnSO (M = Ca or Sr) and (b, c) distribution of the electron clouds around the neighboring atoms. Figure 1c shows that Sr shares the outer shells with the ZnS_3O tetrahedra. Thus, ZnS_3O tetrahedra can be the source of the large birefringence in SrZnSO. Furthermore, Figure 1c shows a high electron density configuration and strong anisotropy for ZnS_3O groups, which indicates the main contribution of the ZnS_3O tetrahedra to the optical anisotropy. It is well known that the birefringence determines partly whether an NLO material has the value of study.

DOI: 10.1021/acs.jpcc.9b08766
J. Phys. Chem. C 2019, 123, 27172−27180

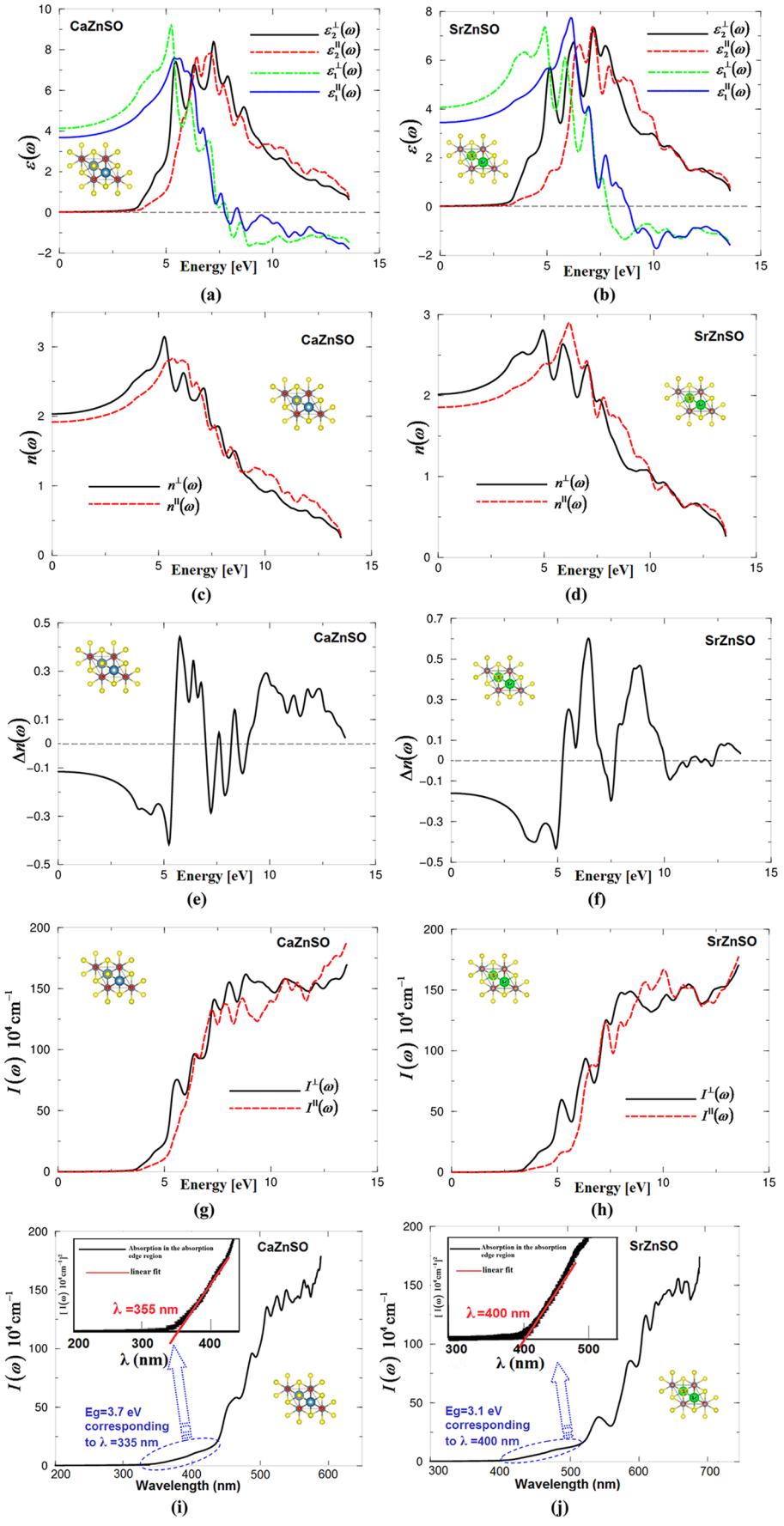

Figure 2. (a, b) Calculated $\varepsilon_2^{\perp}(\omega)$ (dark solid curve, black color online) and $\varepsilon_2^{\mathrm{II}}(\omega)$ (light long dashed curve, red color online) along with calculated $\varepsilon_1^{\perp}(\omega)$ (light dashed curve, green color online) and $\varepsilon_1^{\mathrm{II}}(\omega)$ (dark solid curve, blue color online); (c, d) calculated refractive indices $n^{\perp}(\omega)$ (dark

DOI: 10.1021/acs.jpcc.9b08766
J. Phys. Chem. C 2019, 123, 27172−27180

Figure 2. continued

solid curve, black color online) and $n^{II}(\omega)$ (light dashed curve, red color online); (e, f) calculated birefringence $\Delta n(\omega)$; (g, h) calculated absorption coefficient $I^{\perp}(\omega)$ (dark solid curve, back color online) and $I^{II}(\omega)$ (light dashed curve, red color online), the absorption coefficient in 10^4 cm^{-1}. In semiconductors, the square of the absorption coefficient $I(\omega)$ is linear with energy for direct optical transitions in the absorption edge region. Data plots of MZnSO for $[I(\omega)]^2$ versus wavelength (nm) in the absorption edge region are shown in the inset of Figure 2i,j. The inset show $[I(\omega)]^2$ versus energy is nearly linear. These features suggest that the absorption edges of CaZnSO and SrZnSO are caused by indirect transitions.

Thus, ZnS_3O tetrahedra can be the source of the large birefringence in SrZnSO. Furthermore, a high electron density configuration and strong anisotropy for ZnS_3O groups are evident in Figure 1c, which indicates the main contribution of ZnS_3O tetrahedra to the optical anisotropy.[30] It is well known that the birefringence determines partly whether an NLO material has the value of study.[31−34]

The environment configurations of Sr^{2+} (Ca^{2+}) and Zn^{2+} make both sites highly electrically polar; the noncentrosymmetric distributions of S and O around Sr^{2+} (Ca^{2+}) and Zn^{2+} cations, the equal negative charges of S and O, and the different sizes of S and O force the cations away from their charge barycenters. Therefore, due to spatial restrictions, Sr^{2+} (Ca^{2+}) and Zn^{2+} will move toward the side where the O atoms are situated.[26] Therefore, to investigate the linear and nonlinear optical properties of MZnSO (M = Ca or Sr), ab initio first-principles calculations are performed utilizing the full-potential method (WIEN2k code[35]) within the generalized gradient approximation (PBE-GGA)[36] to optimize the experimental structural geometry of MZnSO (M = Ca or Sr). The obtained structural geometries are used as input data for performing the photophysical properties calculations. The linear and nonlinear optical properties are obtained using the recently modified Becke−Johnson potential (mBJ).[29] The other parameters used in these calculations are the basis functions in the interstitial region and are expanded up to $R_{MT} \times K_{max} = 7.0$ and inside the atomic spheres for the wave function. The $l_{max} = 10$ and the charge density is Fourier-expanded up to $G_{max} = 12$(a. u.)$^{-1}$. The self-consistency is obtained using 4000 k points in the irreducible Brillouin zone (IBZ). The self-consistent calculations are converged since the total energy of the system is stable within 0.00001 Ry. We have used 50,000 k points in the IBZ for calculating the linear and NLO properties. The input required for calculating the linear and NLO properties are the energy eigenvalues and eigenfunctions, which are the natural outputs of a band structure calculation. Therefore, from the band structure calculation, the photophysical properties are calculated. The linear optical properties are calculated using the optical code implemented in the WIEN2k package;[35] for more details, we refer readers to the users' guide[37] and ref 38. The formalism for calculating the nonlinear optical properties is given elsewhere.[39−42]

3. OBTAINED RESULTS AND THE DETAILS DISCUSSION

To investigate the influence of substitution of Ca^{2+} (180 pm) by larger Sr^{2+} (200 pm) in CaZnSO on the structural properties and hence on the linear and nonlinear optical properties, we have performed a comprehensive ab inito calculation. It has been reported that substitution of Ca^{2+} by Sr^{2+} in CaZnSO introduces a different chemical pressure, which can change the structural polarity and the energy band gap resulting in influence on the optical properties.[25] The calculation shows that substitution of Ca^{2+} by Sr^{2+} causes a band gap reduction from 3.7 eV (CaZnSO)[25] to 3.1 eV (SrZnSO),[26] which is in good agreement with the experimental data[25,26] and results in enhancing the optic activity toward the visible region. As the Ca-homologue is proved to be strongly nonlinearly active,[25] thus, it is important to highlight that the Sr homologue is isostructural to the Ca homologue.[26] From the electronic band structure (Figure S1a,b), the spectral features of the complex first-order linear optical dielectric functions are obtained.

The imaginary and real parts of the interband optical dielectric functions for MZnSO (M = Ca or Sr) are shown in Figure 2a,b. The band gap reduction occurs on moving from Ca to Sr, which is in good agreement with the experimental data,[25,26] and the whole spectral structure shifts toward lower energies, indicating that the fundamental absorption edge shifts toward the visible light region. The dispersive part of the optical dielectric functions can give information about the energy gaps since the calculated static electronic dielectric constant $\varepsilon_\infty = \varepsilon_1(0)$ is inversely related to the energy gap, as explained in the Penn model.[43] The dispersive parts of the optical dielectric functions vanish at an energy of about 7.5 eV and present negative values, and this corresponds to the energy loss of a fast electron traversing in the material (Figure S2a,b).

Moreover, as seen in Figure 2a,b, the substitution of Ca^{2+} by Sr^{2+} in CaZnSO induces an obvious enhancement in the anisotropy between the extraordinary and ordinary tensor components. The uniaxial anisotropy ($\delta\varepsilon$) can be calculated from the zero frequency value of the dispersive part of the optical dielectric functions. It is found that both compounds exhibit a negative $\delta\varepsilon$ (Table 1). The enhancement of anisotropy in the linear optical dielectric tensor favors an important quantity in SHG and OPO due to better phase-matching conditions controlled by birefringence. Therefore, we expected that the SrZnSO will exhibit higher SHG than CaZnSO. The birefringence can be obtained from the differences between the extraordinary and ordinary tensor components of the refractive indices (Figure 2c−f). It is clear that both compounds exhibit negative birefringence (Table 1).

Table 1. Calculated Energy Band Gap in Comparison with the Experimental Value

parameter	CaZnSO	SrZnSO
E_g (eV)	3.7, 3.7[a]	3.1, 3.1[b]
$\varepsilon_1^{\perp}(0)$	4.138	4.070
$\varepsilon_1^{II}(0)$	3.681	3.447
$\delta\varepsilon$	−0.116	−0.165
$\omega_p^{\perp}(\omega)$	7.877	7.850
$\omega_p^{\parallel}(\omega)$	7.768	8.830
$n^{\perp}(0)$	2.034	2.017
$n^{II}(0)$	1.918	1.856
$\Delta n(0)$	−0.116	−0.161
$\Delta n(\omega)$ at λ = 1064 nm	−0.121	−0.168

[a]Ref 25 (experimental work). [b]Ref 26 (experimental work).

DOI: 10.1021/acs.jpcc.9b08766
J. Phys. Chem. C 2019, 123, 27172−27180

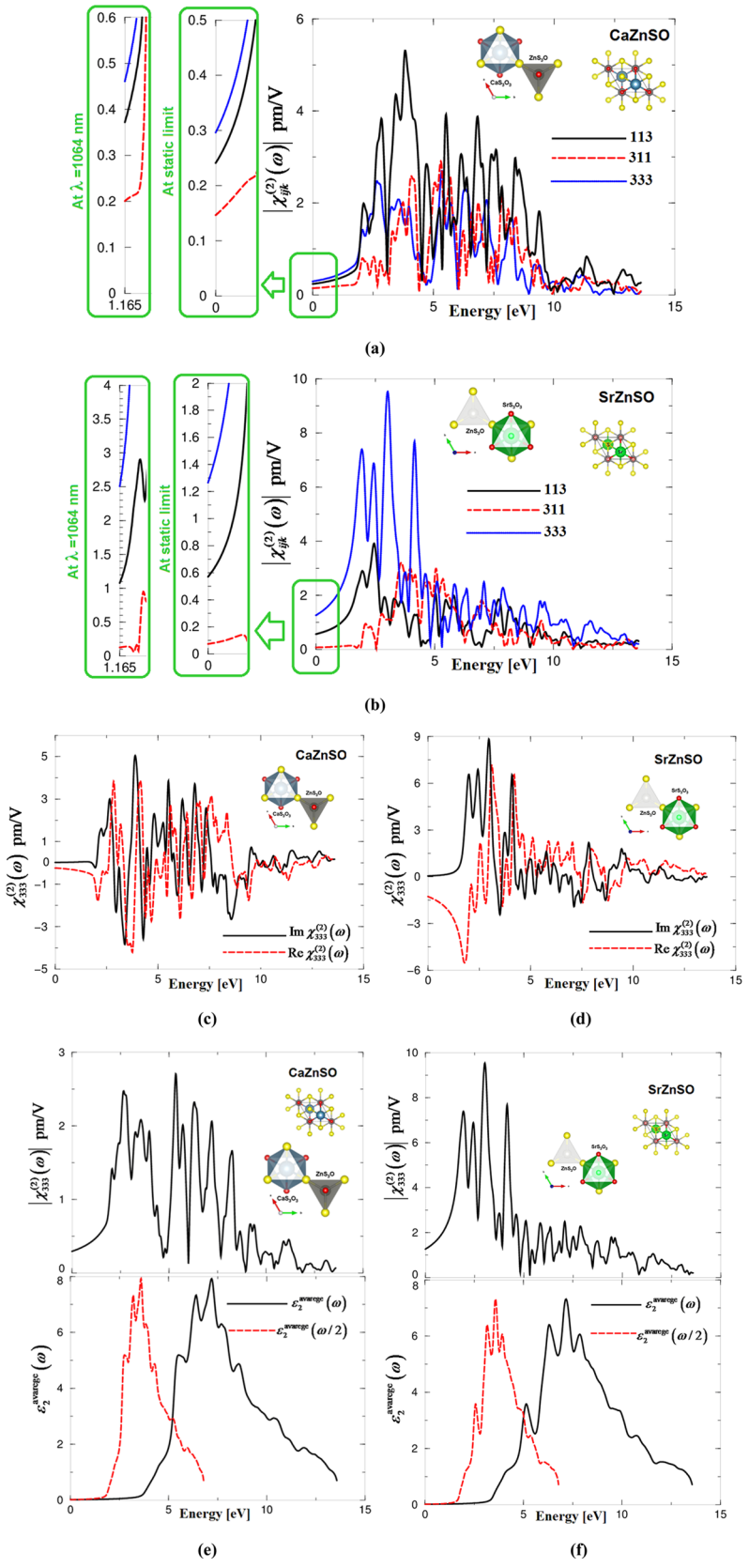

Figure 3. (a, b) Calculated $|\chi^{(2)}_{ijk}(\omega)|$ for the three tensor components; (c, d) calculated total imaginary $\chi^{(2)}_{333}(\omega)$ spectrum (dark solid curve, black color online) and real $\chi^{(2)}_{333}(\omega)$ (light long dashed curve, red color online); (e, f) (upper panel) calculated$|\chi^{(2)}_{333}(\omega)|$ (dark solid curve,black color online) and (lower panel) calculated $\varepsilon_2^{xx}(\omega)$ (dark solid curve, black color online) and calculated $\varepsilon_2^{xx}(\omega/2)$ (dark dashed curve, red color online).

It is well known that the birefringence determines partly whether an NLO material has potential utility.[31]

Furthermore, to investigate the influence of substitution of Ca^{2+} by Sr^{2+} on the optical properties, we have calculated the

DOI: 10.1021/acs.jpcc.9b08766
J. Phys. Chem. C 2019, 123, 27172−27180

Table 2. Calculated $|\chi^{(2)}_{ijk}(\omega)|$ and β_{ijk} of CaZnSO, in pm/V at Static Limit and at λ = 1064 nm[a]

	CaZnSO			
tensor components	$\chi^{(2)}_{ijk}(0)$	$d_{ijk} = 0.5\chi^{(2)}_{ijk}(\omega)$ at static limit	$\chi^{(2)}_{ijk}(\omega)$ at λ = 1064 nm	$d_{ijk} = 0.5\chi^{(2)}_{ijk}(\omega)$ λ = 1064 nm
$\|\chi^{(2)}_{113}(\omega)\|$	0.239	d_{15} = 0.1195	0.371	d_{15} = 0.1855
$\|\chi^{(2)}_{311}(\omega)\|$	0.146	d_{11} = 0.073	0.201	d_{11} = 0.1005
$\|\chi^{(2)}_{333}(\omega)\|$	0.299	d_{33} = 0.1495	0.460	d_{33} = 0.2300
β_{333}	0.0443×10^{-30} esu		0.0694×10^{-30} esu	

[a]Where 1 pm/V = 2.387×10^{-9} esu. It has been found that the obtained value of d_{33} at λ = 1064 nm is about 0.23 pm/V.

Table 3. Calculated $|\chi^{(2)}_{ijk}(\omega)|$ and β_{ijk} of SrZnSO, in pm/V at Static Limit and at λ = 1064 nm[a]

	SrZnSO			
tensor components	$\chi^{(2)}_{ijk}(0)$	$d_{ijk} = 0.5\ \chi^{(2)}_{ijk}(\omega)$ at static limit	$\chi^{(2)}_{ijk}(\omega)$ at λ = 1064 nm	$d_{ijk} = 0.5\ \chi^{(2)}_{ijk}(\omega)$ λ = 1064 nm
$\|\chi^{(2)}_{113}(\omega)\|$	0.574	d_{15} = 0.287	1.101	d_{15} = 0.5505
$\|\chi^{(2)}_{311}(\omega)\|$	0.08	d_{11} = 0.04	0.131	d_{11} = 0.0655
$\|\chi^{(2)}_{333}(\omega)\|$	1.38	d_{33} = 0.66	2.531	d_{33} = 1.2655
β_{333}	0.2062×10^{-30} esu		0.4206×10^{-30} esu	

[a]Where 1 pm/V = 2.387×10^{-9} esu. It has been found that the obtained value of d_{33} at λ = 1064 nm is about 1.27 pm/V, which is almost 1/10 of the experimental value of the well-known $KTiOPO_4$ (KTP) single crystals, which exhibits an SHG value of about 13.7 [ref 47] at λ = 1064 nm.

optical conductivity ($\sigma(\omega) = \frac{4\pi k(\omega)}{\lambda}$), which is directly related to the energy band structure of solids (Figure S1a,b).[44] Therefore, deep insight into the electronic structure of the materials can be further obtained from the $\sigma(\omega)$ (Figure S2c,d). From $\sigma_2(\omega)$, the value of the plasma energy can be obtained, and these are $h\omega_p^{\perp}(\omega)$ = 7.877 (7.850) eV and $h\omega_p^{\parallel}(\omega)$ = 7.768 (8.830) eV. The calculated $\sigma(\omega)$ depicts the conduction induced by the electrons, which move from the valence band to the conduction band upon absorption of incident light. Since $\sigma(\omega)$ appears as a result of absorption, the features of the curves in Figure S2c,d and Figure 2a,b are closely related and the peaks represent optically induced electronic transitions between different states of the occupied valence band and the unoccupied conduction band. The absorption level of CaZnSO (SrZnSO) (Figure 2g−j) exhibited an obvious enhancement in the visible light region, and it shows that the absorption edge shifts from λ = 335 nm (CaZnSO) to 400 nm (SrZnSO), which corresponds to a direct band gap of 3.7 (3.1) eV and well matched with the solar spectrum. In semiconductors, the square of the absorption coefficient $I(\omega)$ is linear with energy for direct optical transitions in the absorption edge region.[45,46] The data plots of MZnSO for $[I(\omega)]^2$ versus wavelength in the absorption edge region are shown in the inset of Figure 2i,j. The inset shows that $[I(\omega)]^2$ versus energy is nearly linear. These features suggest that the absorption edges of CaZnSO and SrZnSO are caused by direct transitions. As evident in Figure S2e,f, where the reflectivity spectra of CaZnSO and SrZnSO are shown, the small value of reflectance 0.10−0.15 in the range of 0.0−3.0 eV ensures the material applications as transparent coatings in the UV and visible regimes.

Based on the calculated electronic band structure, the SHG properties can be obtained using the formalism given elsewhere.[39−42] Since CaZnSO and SrZnSO crystallize in hexagonal symmetry, therefore, only three nonvanish tensor components are completely identifying the SHG. These are $\chi^{(2)}_{131}(\omega) = \chi^{(2)}_{113}(\omega) = \chi^{(2)}_{232}(\omega) = \chi^{(2)}_{223}(\omega)$, $\chi^{(2)}_{311}(\omega) = \chi^{(2)}_{322}(\omega)$, and $\chi^{(2)}_{333}(\omega)$ according to Kleinman's symmetry. The calculated $|\chi^{(2)}_{ijk}(\omega)|$ for CaZnSO and SrZnSO are given in Figure 3a,b, which show considerable anisotropy between the three tensor components. The values of $|\chi^{(2)}_{113}(\omega)|$, $|\chi^{(2)}_{311}(\omega)|$, and $|\chi^{(2)}_{333}(\omega)|$ at static limit and at the wavelength 1064 nm are listed in Tables 2 and 3. Following Figure 3a,b and Tables 2 and 3, one can see that $|\chi^{(2)}_{333}(\omega)|$ is the dominate tensor component, which exhibits bigger value for SrZnSO. It has been found that the obtained value of d_{33} for CaZnSO at λ = 1064 nm is about 0.23 pm/V. While the obtained value of d_{33} for SrZnSO at λ = 1064 nm is about 1.27 pm/V, which almost 1/10 of the experimental value of the well-known $KTiOPO_4$ (KTP) single crystals, which exhibits an SHG value of about 13.7[47] at λ = 1064 nm. It is clear that the SHG of SrZnSO is larger than that of CaZnSO. The relation is attributed to the fact that Sr shares the outer shells with ZnS_3O tetrahedra and it makes this configuration the main source of large birefringence in SrZnSO and, hence, large SHG. As it has been mentioned before, (i) the birefringence determines partly whether an NLO material has potential utility,[31] (ii) the enhancement in the anisotropy in the linear optical dielectric tensor favors an important quantity in SHG due to better fulfilling of phase-matching conditions, determined by birefringence, and (iii) the requirement for obtaining good NLO materials is achieving the delicate balance between the SHG response and energy band gap.[23,48]

Sambrook et al.[25] reported that the SHG value of CaZnSO is approximately 100 times that of α-SiO_2, and we should emphasize that this value is for a powder without taking into account the influence of the packing structural units. Hence, we have calculated the SHG of the CaZnSO and SrZnSO crystals taking into account the influence of the packing structural units. According to the anionic group theory,[27] the overall SHG response of crystal is the geometrical superposition of the second-order susceptibilities. Therefore, the packing structural units may also affect the macroscopic SHG coefficients.[28] The large SHG is due to the strong interactions between the structural units.[28]

The condition for getting good SHG performance is a small energy band gap (CaZnSO > SrZnSO), which limits the transmittance in the ultraviolet (UV) region. Therefore, the requirement for obtaining good NLO materials is achieving the delicate balance between the SHG response and energy band gap.[48] Based on our obtained SHG values, we can say that CaZnSO is a good NLO material in the UV region, whereas SrZnSO is a good NLO material in the visible region.[49−51]

DOI: 10.1021/acs.jpcc.9b08766
J. Phys. Chem. C 2019, 123, 27172−27180

Thus, the substitution of Ca^{2+} by Sr^{2+} in CaZnSO tunes the material to be efficient in the visible region.

Furthermore, to understand the origin of SHG in CaZnSO and SrZnSO, the imaginary and real parts of the dominate tensor component are investigated, as shown in Figure 3c,d. The influence of the packing structural units (Figure 1) on the spectral features of the imaginary and real parts of $\chi^{(2)}_{333}(\omega)$ is clearly shown. Therefore, the substitution of Ca^{2+} by Sr^{2+} causes a significant influence on the resulting SHG, which is attributed to the fact that the NLO properties are more sensitive to small changes in the band structure than the linear optical properties. Figure S2g,h illustrates the contributions of the 2ω and ω inter/intraband transitions. It is clear that the 2ω inter/intraband transitions in CaZnSO (SrZnSO) start to oscillate at energy values of about 1.85 (1.55) eV, whereas the ω inter/intraband transitions oscillate at 3.7 (3.1) eV, the value of the fundamental energy band gap. To gain more details concerning the origin of the spectral features of the SHG, the absolute value of the dominate tensor component $|\chi^{(2)}_{333}(\omega)|$ is compared to the spectral features of $\varepsilon_2(\omega)$ and $\varepsilon_2(\omega/2)$, as shown in Figure 3e,f. Due to the presence of 2ω term in the spectral structure of $|\chi^{(2)}_{333}(\omega)|$ that makes it difficult to use the electronic band structure to identify the origin of the spectral features in $|\chi^{(2)}_{333}(\omega)|$ therefore, we have associated the spectral features of $\varepsilon_2(\omega)$ and $\varepsilon_2(\omega/2)$ with $|\chi^{(2)}_{333}(\omega)|$ for better understanding. The spectral features of $|\chi^{(2)}_{333}(\omega)|$ in CaZnSO (SrZnSO) between 1.85 (1.55) eV and 3.7 (3.1) eV are formed by the 2ω resonance only, whereas the spectral features of $|\chi^{(2)}_{333}(\omega)|$ in the energy region between 3.7(3.1) eV and 7.0 eV come from the 2ω and ω resonance. The spectral structure from 7.0 eV to 14.0 eV is formed from the ω resonance only. Furthermore, from the calculated values of $\chi^{(2)}_{113}(\omega)$, $\chi^{(2)}_{311}(\omega)$, and $\chi^{(2)}_{333}(\omega)$, the microscopic first hyperpolarizability, β_{ijk},[52,53] the vector component along the dipole moment direction, can be obtained (Tables 2 and 3).

In the recent years, due to the improvement of the computational technologies, it has been proven that the first-principles calculation is a strong and useful tool to predict the crystal structure and properties related to the electron configuration of a material before its synthesis.[45,46,54−56]

4. SUMMARY

Using the reported X-ray diffraction data reported by Sambrook et al. for CaZnSO and Lin et al. for SrZnSO, a comprehensive ab inito calculation is performed to investigate the influence of substitution of Ca^{2+} by Sr^{2+} on the structural properties and, hence, on the linear and nonlinear optical properties. The calculation reveals a band gap reduction toward the visible region on moving from Ca to Sr, which is in good agreement with the previous experimental data. The enhanced anisotropy (Ca → Sr) favors an important quantity in second harmonic generation (SHG) and optical parameter oscillator (OPO) due to better fulfilling of phase-matching conditions. The substitution of Ca by larger Sr causes an influence on the bond lengths, and this may lead to an influence on the electronic properties. The calculation shows that SrZnSO exhibits larger SHG and β_{ijk} than CaZnSO.

■ ASSOCIATED CONTENT

Supporting Information

The Supporting Information is available free of charge on the ACS Publications website at DOI: 10.1021/acs.jpcc.9b08766.

Figure S1: calculated electronic band structure of sulfide oxide MZnSO (M = Ca or Sr); Figure S2: (a, b) calculated loss function $L^{\perp}(\omega)$ (dark solid curve, black color online) and $L^{\text{II}}(\omega)$ (light dashed curve, red color online); (c, d) calculated $\sigma_2^{\perp}(\omega)$ (dark solid curve, black color online) and $\sigma_2^{\text{II}}(\omega)$ (light dashed curve, red color online) along with calculated $\sigma_1^{\perp}(\omega)$ (dark solid curve, blue color online) and $\sigma_1^{\text{II}}(\omega)$ (light dashed curve, red online); (e, f) calculated $R^{\perp}(\omega)$ (dark solid curve, black color online) and $R^{\text{II}}(\omega)$ (light dashed curve, red color online); (e, f) calculated total $\text{Im}\chi^{(2)}_{333}(\omega)$ spectrum (dark solid curve, black color online) along with the intraband $(2\omega)/(1\omega)$ (light solid curve, blue color online)/(light dashed doted curve, cyan color online) and interband $(2\omega)/(1\omega)$ (light long dashed curve, red color online)/(light doted curve, green color online) contributions (PDF)

■ AUTHOR INFORMATION

Corresponding Author

*E-mail: maalidph@yahoo.co.uk.

ORCID

Ali H. Reshak: 0000-0001-9426-8363

Notes

The authors declare no competing financial interest.

■ REFERENCES

(1) Becker, P. Borate materials in nonlinear optics. *Adv. Mater.* **1998**, *10*, 979−992.

(2) Sasaki, T.; Mori, Y.; Yoshimura, M.; Yap, Y. K.; Kamimura, T. Recent development of nonlinear optical borate crystals: key materials for generation of visible and UV light. *Mater. Sci. Eng., R* **2000**, *30*, 1−54.

(3) Halasyamani, P. S.; Poeppelmeier, K. R. Noncentrosymmetric Oxides. *Chem. Mater.* **1998**, *10*, 2753−2769.

(4) Chen, C.; Lin, Z.; Wang, Z. The development of new borate-based UV nonlinear optical crystals. *Appl. Phys. B: Lasers Opt.* **2005**, *80*, 1−25.

(5) Belokoneva, E. L. Borate crystal chemistry in terms of the extended OD theory: Topology and symmetry analysis. *Crystallogr. Rev.* **2005**, *11*, 151−198.

(6) Pan, S.; Smit, J. P.; Watkins, B.; Marvel, M. R.; Stern, C. L.; Poeppelmeier, K. R. Synthesis, crystal structure, and nonlinear optical properties of $Li_6CuB_4O_{10}$: A congruently melting compound with isolated $[CuB_4O_{10}]$ 6- units. *J. Am. Chem. Soc.* **2006**, *128*, 11631−11634.

(7) Chi, E. O.; Ok, K. M.; Porter, Y.; Halasyamani, P. S. $Na_2Te_3Mo_3O_{16}$: A New Molybdenum Tellurite with Second-Harmonic Generating and Pyroelectric Properties. *Chem. Mater.* **2006**, *18*, 2070−2074.

(8) Pan, S.; Wu, Y.; Fu, P.; Zhang, G.; Li, Z.; Du, C.; Chen, C. Growth, structure, and properties of single crystals of $SrBPO_5$. *Chem. Mater* **2003**, *15*, 2218−2221.

(9) Hu, Z. G.; Yoshimura, M.; Mori, Y.; Sasaki, T. Design and growth of new NLO crystals for UV light generation. *J. Cryst. Growth* **2005**, *275*, 232−239.

(10) Wang, S.; Ye, N.; Li, W.; Zhao, D. Alkaline beryllium borate NaBeB3O6 and ABe(2)B(3)O(7) (A = K, Rb) as UV nonlinear optical crystals. *J. Am. Chem. Soc.* **2010**, *132*, 8779−8786.

(11) Pan, S.; Smit, J. P.; Lanier, C. H.; Marvel, M. R.; Marks, L. D.; Poeppelmeier, K. R. Optical floating zone growth of β-BaB_2O_4 from a $LiBa_2B_5O_{10}$-based solvent. *Cryst. Growth Des.* **2007**, *7*, 1561−1564.

(12) Goodey, J.; Broussard, J.; Halasyamani, P. S. Synthesis, Structure, and Characterization of a New Second-Harmonic-

DOI: 10.1021/acs.jpcc.9b08766
J. Phys. Chem. C 2019, 123, 27172−27180

Generating Tellurite: $Na_2TeW_2O_9$. *Chem. Mater.* **2002**, *14*, 3174−3180.
(13) Li, F.; Hou, X.; Pan, S.; Wang, X. Growth, structure, and optical properties of a congruent meltingoxyborate, $Bi_2ZnOB_2O_6$. *Chem. Mater.* **2009**, *21*, 2846−2850.
(14) Kong, F.; Huang, S. P.; Sun, Z. M.; Mao, J. G.; Cheng, W. D. $Se_2(B_2O_7)$: a new type of second-order NLO material. *J. Am. Chem. Soc.* **2006**, *128*, 7750−7751.
(15) Chen, C.; Wang, Y.; Wu, B.; Wu, K.; Zeng, W.; Yu, L. Design and synthesis of an ultraviolet-transparent nonlinear optical crystal $Sr_2Be_2B_2O_7$. *Nature* **1995**, *373*, 322−324.
(16) Fan, X.; Pan, S.; Hou, X.; Tian, X.; Han, J. Growth and Properties of Single Crystals of Noncentrosymmetric $Na_3VO_2B_6O_{11}$. *Cryst. Growth Des.* **2010**, *10*, 252−256.
(17) Atuchin, V. V.; Subanakov, A. K.; Aleksandrovsky, A. S.; Bazarov, B. G.; Bazarova, J. G.; Gavrilova, T. A.; Krylov, A. S.; Molokeev, M. S.; Oreshonkov, A. S.; Stefanovich, S. Y. Structural and spectroscopic properties of new noncentrosymmetric self-activated borate $Rb_3EuB_6O_{12}$ with B_5O_{10} units. *Mater. Des.* **2018**, *140*, 488−494.
(18) Chen, C. T. Recent advances in deep and vacuum-UV harmonic generation with KBBF crystal. *Opt. Mater.* **2004**, *26*, 425−429.
(19) Lin, J.; Lee, M.-H.; Liu, Z.-P.; Chen, C.; Pickard, C. J. Mechanism for linear and nonlinear optical effects in β−BaB_2O_4 crystals. *Phys. Rev. B* **1999**, *60*, 13380.
(20) Chen, C.; Wu, Y.; Jiang, A.; Wu, B.; You, G.; Li, R.; Lin, S. New nonlinear-optical crystal: LiB_3O_5. *J. Opt. Soc. Am. B* **1989**, *6*, 616−621.
(21) Kang, L.; Lin, Z.; Qin, J.; Chen, C. Two novel nonlinear optical carbonates in the deep-ultraviolet region: $KBeCO_3F$ and $RbAlCO_3F_2$. *Sci. Rep.* **2013**, *3*, 1366.
(22) Zou, G.; Ye, N.; Huang, L.; Lin, X. Alkaline-alkaline earth fluoride carbonate crystals $ABCO_3F$ (A = K, Rb, Cs; B = Ca, Sr, Ba) as nonlinear optical materials. *J. Am. Chem. Soc.* **2011**, *133*, 20001−20007.
(23) Liang, F.; Kang, L.; Lin, Z.; Wu, Y.; Chen, C. Analysis and prediction of mid-IR nonlinear optical metal sulfides with diamond-like structures. *Coord. Chem. Rev.* **2017**, *333*, 57−70.
(24) Lin, Z.; Jiang, X.; Kang, L.; Gong, P.; Luo, S.; Lee, M.-H. First-principles materials applications and design of nonlinear optical crystals. *J. Phys. D: Appl. Phys.* **2014**, *47*, 253001.
(25) Sambrook, T.; Smura, C. F.; Clarke, S. J.; Ok, K. M.; Halasyamani, P. S. Structure and Physical Properties of the Polar Oxysulfide CaZnOS. *Inorg. Chem.* **2007**, *46*, 2571−2574.
(26) Liu, W.; Lai, K. T.; Eckhardt, K.; Prots, Y.; Burkhardt, U.; Valldor, M. Synthesis and characterization of sulfide oxide SrZnSO with strongly polar crystal structure. *J. Solid State Chem.* **2017**, *246*, 225−229.
(27) Chen, C.; Wu, Y.; Li, R. The anionic group theory of the non-linear optical effect and its applications in the development of new high-quality NLO crystals in the borate series. *Int. Rev. Phys. Chem.* **1989**, *8*, 65−91.
(28) Abudoureheman, M.; Wang, L.; Zhang, X.; Yu, H.; Yang, Z.; Lei, C.; Han, J.; Pan, S. $Pb_7O(OH)_3(CO_3)_3(BO_3)$: First Mixed Borate and Carbonate Nonlinear Optical Material Exhibiting Large Second-Harmonic Generation Response. *Inorg. Chem.* **2015**, *54*, 4138−4142.
(29) Tran, F.; Blaha, P. Accurate Band Gaps of Semiconductors and Insulators with a Semilocal Exchange-Correlation Potential. *Phys. Rev. Lett.* **2009**, *102*, 226401.
(30) Lei, B.-H.; Yang, Z.; Pan, S. Enhancing optical anisotropy of crystals by optimizing bonding electron distribution in anionic groups. *Chem. Commun.* **2017**, *53*, 2818−2821.
(31) Bian, Q.; Yang, Z.; Dong, L.; Pan, S.; Zhang, H.; Wu, H.; Yu, H.; Zhao, W.; Jing, Q. First Principle Assisted Prediction of the Birefringence Values of Functional Inorganic Borate Materials. *J. Phys. Chem. C* **2014**, *118*, 25651−25657.
(32) Andreev, Y. M.; Atuchin, V. V.; Lanskii, G. V.; Pervukhina, N. V.; Popov, V. V.; Trocenco, N. C. Linear optical properties of LiIn(S1-xSex)2 crystals and tuning of phase matching conditions. *Solid State Sci.* **2005**, *7*, 1188−1193.
(33) Kang, Z.-H.; Guo, J.; Feng, Z.-S.; Gao, J.-Y.; Xie, J.-J.; Zhang, L.-M.; Atuchin, V.; Andreev, Y.; Lanskii, G.; Shaiduko, A. Tellurium and sulfur doped GaSe for mid-IR applications. *Appl. Phys. B* **2012**, *108*, 545−552.
(34) Atuchin, V. V.; Adichtchev, S. V.; Bazarov, B. G.; Bazarova, Z. G.; Gavrilova, T. A.; Grossman, V. G.; Kesler, V. G.; Meng, G. S.; Lin, Z. S.; Surovtsev, N. V. Electronic structure and vibrational properties of $KRbAl_2B_2O_7$. *Mater. Res. Bull.* **2013**, *48*, 929−934.
(35) Blaha, P.; Schwarz, K.; Madsen, G. K. H.; Kvasnicka, D.; Luitz, J. *WIEN2k, An augmented plane wave plus local orbitals program for calculating crystal properties*; Vienna University of Technology: Austria, 2001.
(36) Perdew, J. P.; Burke, K.; Ernzerhof, M. Generalized Gradient Approximation Made Simple. *Phys. Rev. Lett.* **1996**, *77*, 3865.
(37) http://www.wien2k.at/reg_user/textbooks/usersguide.pdf
(38) Ambrosch-Draxl, C.; Sofo, J. O. Linear optical properties of solids within the full-potential linearized augmented planewave method. *Comput. Phys. Commun.* **2006**, *175*, 1−14.
(39) Sharma, S.; Dewhurst, J. K.; Ambrosch-Draxl, C. Linear and second-order optical response of III-V monolayer superlattices. *Phys. Rev. B* **2003**, *67*, 165332.
(40) Ph.D. thesis, Reshak, A. H. Indian Institute of Technology-Rookee; India (2005).
(41) Reshak, A. H. Electronic, linear, and nonlinear optical properties of III-V indium compound semiconductors. *J. Chem. Phys.* **2006**, *125*, No. 034710.
(42) Reshak, A. H. Theoretical investigation of the electronic properties, and first and second harmonic generation for cadmium chalcogenide. *J. Chem. Phys.* **2006**, *124*, 104707.
(43) Penn, D. R. Wave-Number-Dependent Dielectric Function of Semiconductors. *Phys. Rev. B* **1962**, *128*, 2093.
(44) Dresselhaus, M. S. *Solid State Physics Part II Optical Properties of Solids*. http://web.mit.edu/afs/athena/course/6/6.732/www/opt.pdf, 2001.
(45) Huang, H.; He, Y.; Li, X.; Li, M.; Zeng, C.; Dong, F.; Du, X.; Zhang, T.; Zhang, Y. $Bi_2O_2(OH)(NO_3)$ as a desirable $[Bi_2O_2]^{2+}$ layered photocatalyst: strong intrinsic polarity, rational band structure and {001} active facets co-beneficial for robust photooxidation capability. *J. Mater. Chem. A* **2015**, *3*, 24547−24556.
(46) Huang, H.; He, Y.; Lin, Z.; Kang, L.; Zhang, Y. Two Novel Bi-Based Borate Photocatalysts: Crystal Structure, Electronic Structure, Photoelectrochemical Properties, and Photocatalytic Activity under Simulated Solar Light Irradiation. *J. Phys. Chem. C* **2013**, *117*, 22986−22994.
(47) *Potassium Titanyl Phosphate ($KTiOPO_4$,KTP)*. http://www.castech-us.com/casktp.htm.
(48) Li, D.; Jing, Q.; Lei, C.; Pan, S.; Zhang, B.; Yang, Z. Theoretical perspective of the lone pair activity influence on band gap and SHG response of lead borates. *RSC Adv.* **2015**, *5*, 79882−79887.
(49) Zhang, B.; Shi, G.; Yang, Z.; Zhang, F.; Pan, S. Fluorooxoborates: Beryllium-Free Deep-Ultraviolet Nonlinear Optical Materials without Layered Growth. *Angew. Chem., Int. Ed.* **2017**, *56*, 3916−3919.
(50) Yang, Z.; Lei, B.-H.; Zhang, W.; Pan, S. Module-Analysis-Assisted Design of Deep Ultraviolet Fluorooxoborates with Extremely Large Gap and High Structural Stability. *Chem. Mater.* **2019**, *31*, 2807−2813.
(51) Shi, G.; Wang, Y.; Zhang, F.; Zhang, B.; Yang, Z.; Hou, X.; Pan, S.; Poeppelmeier, K. R. Finding the Next Deep-Ultraviolet Nonlinear Optical Material: NH4B4O6F. *J. Am. Chem. Soc.* **2017**, *139*, 10645−10648.
(52) Boyd, R. Y. *Principles of Nonlinear Optics*; Academic Press: NY, 1982, 420.
(53) Boyd, R. W. *Nonlinear optics*; third *edition*, 2008, Academic Press is an imprint of Elsevier: ISBN:978−0−12-369470-6
(54) Davydyuk, G. E.; Khyzhun, O. Y.; Reshak, A. H.; Kamarudin, H.; Myronchuk, G. L.; Danylchuk, S. P.; Fedorchuk, A. O.; Piskach, L.

DOI: 10.1021/acs.jpcc.9b08766
J. Phys. Chem. C 2019, 123, 27172−27180

V.; Mozolyuk, M. Y.; Parasyuk, O. V. Photoelectrical properties and the electronic structure of $Tl_{1-x}In_{1-x}Sn_xSe_2$ (x = 0, 0.1, 0.2, 0.25) single crystalline alloys. *Phys. Chem. Chem. Phys.* **2013**, *15*, 6965.

(55) Zhang, J.; Yu, W.; Liu, J.; Liud, B. Illustration of high-active Ag_2CrO_4 photocatalyst from the first-principle calculation of electronic structures and carrier effective mass. *Appl. Surf. Sci.* **2015**, *358*, 457−462.

(56) Li, X.; Zhao, J.; Yang, J. Semihydrogenated BN Sheet: A Promising Visible-light Driven Photocatalyst for Water Splitting. *Sci. Rep.* **2013**, *3*, 1858.

DOI: 10.1021/acs.jpcc.9b08766
J. Phys. Chem. C 2019, 123, 27172−27180